Fast-diffusing p75^{NTR} monomers support apoptosis and growth cone collapse by neurotrophin ligands

Laura Marchetti[a,b,c,d,1,2], Fulvio Bonsignore[a,1], Francesco Gobbo[b,e,1], Rosy Amodeo[a,c], Mariantonietta Calvello[b], Ajesh Jacob[b], Giovanni Signore[a,c,3], Chiara Schirripa Spagnolo[a], David Porciani[a,c,4], Marco Mainardi[b], Fabio Beltram[a,3], Stefano Luin[a,f,2,5], and Antonino Cattaneo[b,2,5]

[a]National Enterprise for NanoScience and NanoTechnology (NEST) Laboratory, Scuola Normale Superiore, 56127 Pisa, Italy; [b]Bio@SNS, Scuola Normale Superiore, 56124 Pisa, Italy; [c]Center for Nanotechnology Innovation @NEST, Istituto Italiano di Tecnologia, 56127 Pisa, Italy; [d]Dipartimento di Farmacia, Università di Pisa, 56126 Pisa, Italy; [e]Centre for Discovery Brain Sciences, University of Edinburgh, Edinburgh EH8 9JZ, United Kingdom; and [f]NEST, Istituto di Nanoscienze, Consiglio Nazionale delle Ricerche, 56127 Pisa, Italy

Edited by K. Christopher Garcia, Stanford University, Stanford, CA, and approved August 14, 2019 (received for review February 17, 2019)

The p75 neurotrophin (NT) receptor (p75^{NTR}) plays a crucial role in balancing survival-versus-death decisions in the nervous system. Yet, despite 2 decades of structural and biochemical studies, a comprehensive, accepted model for p75^{NTR} activation by NT ligands is still missing. Here, we present a single-molecule study of membrane p75^{NTR} in living cells, demonstrating that the vast majority of receptors are monomers before and after NT activation. Interestingly, the stoichiometry and diffusion properties of the wild-type (wt) p75^{NTR} are almost identical to those of a receptor mutant lacking residues previously believed to induce oligomerization. The wt p75^{NTR} and mutated (mut) p75^{NTR} differ in their partitioning in cholesterol-rich membrane regions upon nerve growth factor (NGF) stimulation: We argue that this is the origin of the ability of wt p75^{NTR} , but not of mut p75^{NTR}, to mediate immature NT (proNT)-induced apoptosis. Both p75^{NTR} forms support proNT-induced growth cone retraction: We show that receptor surface accumulation is the driving force for cone collapse. Overall, our data unveil the multifaceted activity of the p75^{NTR} monomer and let us provide a coherent interpretative frame of existing conflicting data in the literature.

p75 neurotrophin receptor | membrane oligomeric state | single-molecule microscopy | apoptosis | growth cone collapse

The p75 neurotrophin (NT) receptor (p75^{NTR}) is a single-pass transmembrane (TM) receptor of the tumor necrosis factor (TNF) receptor superfamily (1). Along with the Trk tyrosine kinase receptor (2) and the Vps10p domain-sorting receptor families (3), p75^{NTR} binds and is activated by NTs, small secreted homodimeric growth factors. NTs regulate survival, differentiation, and specification in developing neurons and plasticity and maintenance in adult neurons (4). This paradigmatic signaling system finely orchestrates 2 opposite pathways—survival versus death—in the central and peripheral nervous systems, and its alterations have a causal role in neurodegeneration (5, 6). Notably, p75^{NTR} is the only NT receptor with significant binding affinity for all NTs, as well as for their respective immature forms (proNTs) (1), thus playing a central role in their balance. The p75^{NTR} has long been considered a pan-NT coreceptor of Trk receptors, cooperating in the formation of high-affinity binding sites for NTs (7). However, the predicted ternary complex between NTs, Trk (or sorting receptors), and p75^{NTR} has never been observed with structural biology techniques, and the available crystal structures of the nerve growth factor (NGF)-TrkA (8) [and NGF-SorC2 (9)], NT–p75^{NTR} binary complexes have opposite orientations: This casts doubts on how a ternary complex could assemble (10). Available NT-p75^{NTR} structures are conflicting per se, as the NGF-p75^{NTR} cocrystal has 2:1 stoichiometry (11), while the NT3-p75^{NTR} cocrystal has 2:2 stoichiometry (12), with no obvious rationale for their difference. In addition, p75^{NTR} binds a number of ligands unrelated to NTs and has independent functions from Trks in controlling neurite outgrowth and morphology (13, 14), cell cycle withdrawal of developing neural progenitors (15), and viral-related neuropathies (16). It is thus clear that the structural basis of p75^{NTR} signaling still needs proper understanding. On the basis of Western blot analysis from cell lysates, it was proposed that p75^{NTR} acts as a preformed disulfide-linked dimer via a conserved TM cysteine residue (Cys256 in human numbering, employed throughout this paper, corresponding to residues 257 in rat and 259 in mouse numberings), which would act as a fulcrum to propagate a conformational change from the p75^{NTR} extra- to intracellular domain upon NT binding (17). Cys256 mutation abolished NT-dependent apoptotic activity in cultured neurons and in a knock-in mouse model (18); however, this model was recently challenged by the report that this propagation of conformational changes could not be supported by the flexible p75^{NTR} juxtamembrane (JM) intracellular region (19). Furthermore, a similar Western blot analysis performed by Anastasia et al. (20) showed the existence of p75^{NTR} trimers, which are more represented than

Significance

Neurotrophins (NTs) are homodimeric growth factors displaying fundamental roles in the nervous system. Their activity stems from binding and activation of 3 different receptor types in nervous cell membranes. The p75 NT receptor (p75^{NTR}) was the first to be discovered in 1986; nevertheless, for the numerous structural and functional facets so far reported, its activation mechanisms have remained elusive. Here, we demonstrate that its pleiotropic functions are regulated by different redistributions of the receptors, which crucially depend on the available NT and on the involved subcellular compartment but are unrelated to its oligomerization state. Single-particle studies proved receptors to be monomers with a fast-diffusive behavior in the membrane with, at most, transient self-interactions on the millisecond time scale.

Author contributions: L.M., F. Bonsignore, F.G., F. Beltram, S.L., and A.C. designed research; L.M., F. Bonsignore, F.G., R.A., A.J., D.P., and M.M. performed research; M.C., G.S., and C.S.S. contributed new reagents/analytic tools; L.M., F. Bonsignore, F.G., R.A., F. Beltram, S.L., and A.C. analyzed data; and L.M., F. Bonsignore, F.G., F. Beltram, S.L., and A.C. wrote the paper.

The authors declare no conflict of interest.

This article is a PNAS Direct Submission.

See Commentary on page 21343.

[1]L.M., F. Bonsignore, and F.G. contributed equally to this work.

[2]To whom correspondence may be addressed. Email: laura.marchetti@unipi.it, s.luin@sns.it, or antonino.cattaneo@sns.it.

[3]Present address: Fondazione Pisana per la Scienza, 56017 S. Giuliano Terme, Pisa, Italy.

[4]Present address: Department of Molecular Microbiology & Immunology, University of Missouri, Columbia, MO 65212.

[5]S.L. and A.C. contributed equally to this work.

This article contains supporting information online at www.pnas.org/lookup/suppl/doi:10.1073/pnas.1902790116/-/DCSupplemental.

First published September 12, 2019.

dimers; oligomerization, however, was not necessary for proNGF-induced growth cone collapse in developing neurons (20).

Here, we directly and quantitatively assess $p75^{NTR}$ oligomerization status in the plasma membrane of living cells by means of single-molecule fluorescence microscopy with a minimally invasive strategy (21, 22); this relies on insertion of a short peptide tag in the $p75^{NTR}$ protein and its labeling with 1:1 stoichiometry (23, 24). This method also allows imaging the receptor with small organic dyes, which, unlike the more cumbersome Quantum dots (Qdot), permits one to retrieve the receptor oligomeric state from their fluorescent intensity (21). We show that membrane $p75^{NTR}$ is mostly a fast-diffusing monomer, regardless of NT stimulation. Its self-interactions are far too transient to result in substantial receptor di- or trimerization; importantly, they do not depend on Cys256 or on other residues previously suggested to play a role in receptor oligomerization. We also gather evidence on why the $p75^{NTR}$ C256A mutant does not elicit NT-dependent apoptosis (18) but is functional for growth cone collapse signaling (20). By solving this apparent contradiction, we revisit here $p75^{NTR}$ function, in the conceptual framework of a versatile monomeric receptor.

Results

Expression, Validation, and Membrane Fluorolabeling of Human $p75^{NTR}$ Constructs. We previously demonstrated that $p75^{NTR}$ can be enzymatically labeled with small chemical probes (e.g., biotin, organic fluorophores) in a site-specific way, inserting 12 amino acid-long tags of the ACP/PCP family at its N terminus (23). This allows a covalent modification with 1:1 stoichiometry (i.e., 1 probe per $p75^{NTR}$ molecule) of the receptors exposed on the surface of living cells (24, 25). Here, we used S6-$p75^{NTR}$ (Fig. 1*A*) for its better labeling performance when compared with A1-$p75^{NTR}$ (*SI Appendix*, Fig. S1). We found that S6-$p75^{NTR}$ correctly localizes on the plasma membrane, as well as on intracellular structures like the nuclear envelope, similar to endogenous $p75^{NTR}$ expressed by PC12 cells (26) (Fig. 1*B*). Like endogenous $p75^{NTR}$ (*SI Appendix*, Fig. S2), S6-$p75^{NTR}$ undergoes palmitoylation (Fig. 1*C*), an important posttranslational modification for $p75^{NTR}$ death domain signaling capability (27). The $p75^{NTR}$ was recently reported to localize asymmetrically in neurons, helping in specifying the future axon (28); accordingly, biotinylated S6-$p75^{NTR}$ receptors preferentially localize in neurites and growth cones in developing hippocampal neurons (Fig. 1*D*). Furthermore, S6-$p75^{NTR}$–EGFP was able to induce growth cone collapse in the same neurons upon proNGF administration (Fig. 1*E*), as reported for previous $p75^{NTR}$ constructs devoid of chemical tags (29). Finally, proBDNF binding to $p75^{NTR}$ was recently reported to increase the number of apoptotic neurons (18) (Fig. 1*F*, *Top*). By transducing S6-$p75^{NTR}$ in cortical neurons from $p75^{NTR}$ knockout (KO) mice (30) with an inducible lentiviral vector (24), we found that it was able to recapitulate proBDNF-induced apoptosis (Fig. 1*F*, *Middle* and *Bottom*). The lower percentage of apoptotic neurons, with respect to that raised by endogenous $p75^{NTR}$, is likely due to the presence of untransduced neurons.

Overall, our data demonstrate that the S6-tagged construct of human $p75^{NTR}$ retains the properties of endogenous $p75^{NTR}$. We therefore employed it to visualize the $p75^{NTR}$ membrane pool in living cells and to describe its behavior in a direct, unperturbed physiological way.

$p75^{NTR}$ Single Molecules Diffuse as Monomers in the Cell Membrane. We first sought to investigate the membrane $p75^{NTR}$ diffusive properties and oligomerization state in living cells. To this end, we expressed S6-$p75^{NTR}$ in neuroblastoma SK-N-BE(2) cells, a line that conceivably models a neuronal membrane with the advantage of lacking endogenous $p75^{NTR}$ and TrkA at both messenger RNA and protein levels (31). Once labeled with

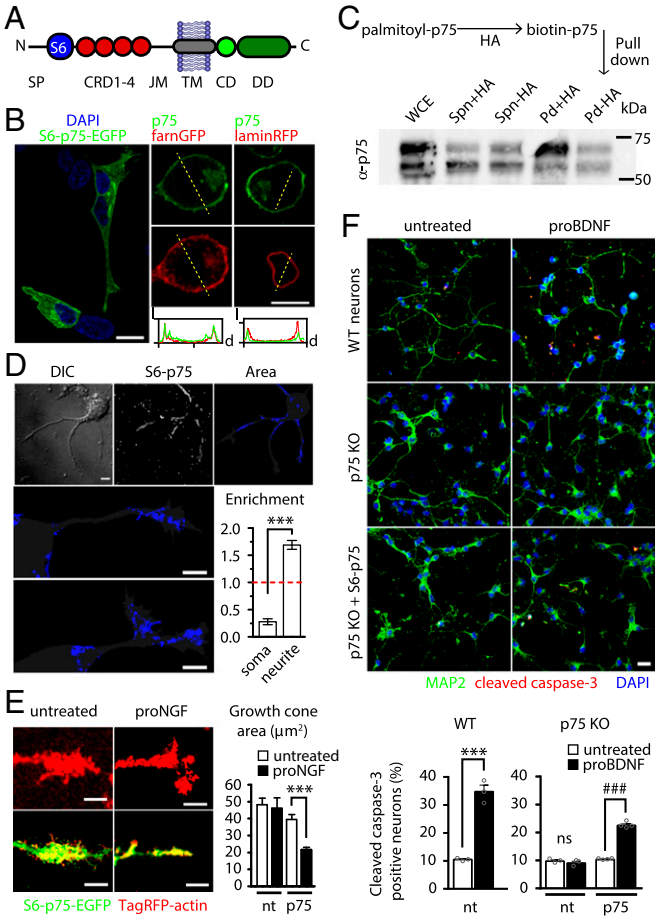

Fig. 1. Expression, validation, and membrane fluorolabeling of human $p75^{NTR}$ constructs. (*A*) Scheme of the S6-$p75^{NTR}$ construct. The S6 tag is inserted between the signal peptide (SP) and cysteine-rich domains 1 to 4 (CRD1-4). CD, chopper; DD, death domain. (*B*) S6-$p75^{NTR}$–EGFP (green) localizes in the plasma membrane and, to a minor extent, on the nuclear membrane in SHSY5Y cells (*Left*) as endogenous $p75^{NTR}$ (green, *Top Right*) in PC12 cells expressing farnesyl (farn)-GFP or lamin-RFP (both red, *Right*). (*Bottom Right*) Intensity (I) vs. distance (d) plot along yellow dashed lines. (Scale bar, 10 μm.) (*C*) S6-$p75^{NTR}$ is palmitoylated. (*Top*) Scheme of the hydroxylamine (HA)-catalyzed palmitoyl/biotin exchange. (*Bottom*) Western blot showing the streptavidin pulldown (Pd) and the corresponding nonpalmitoylated/biotinylated supernatant (Spn); the control reaction without HA is also shown. WCE, whole cell extract. (*D*) S6-$p75^{NTR}$ is polarized in developing hippocampal neurons. The maximum intensity projection of a TIRF movie of Qdot-labeled S6-$p75^{NTR}$ (white) and the area explored by S6-$p75^{NTR}$ (blue) superimposed on the cell mask (gray) are shown. DIC, differential interference contrast. (Scale bars, 5 μm.) The graph shows the relative enrichment in the explored area in somas and neurites. ***$P < 0.001$, paired Student's *t* test (2-tailed). Bars are mean ± SEM. The dotted red line is the value expected for a nonpolarized localization. (*E*, *Left*) Confocal images of growth cones of hippocampal neurons transfected with TagRFP-actin only (red, *Top*) or with S6-$p75^{NTR}$ (green) and TagRFP-actin (*Bottom*), untreated or after 30 min of incubation with 20 ng/mL proNGF. (Scale bars, 5 μm.) (*E*, *Right*) Quantification of the growth cone area is reported in the graph. Bars are mean ± SEM. ***$P < 0.001$, 1-way ANOVA (Bonferroni multiple comparisons). nt, nontransfected. (*F*, *Top*) Cleaved-caspase-3 (red)/MAP2 (green) immunofluorescence images to quantify proBDNF-induced apoptosis in cortical neurons from wt and p75 KO mice (DAPI is shown in blue). (Scale bar, 20 μm.) (*F*, *Bottom*) Percentage of cleaved caspase-3–positive neurons is reported as mean ± SEM in the graph. ***$P < 0.001$, unpaired Student's *t* test (2-tailed); ###$P < 0.001$, 1-way ANOVA (Tukey's multiple comparisons). ns, not significant at the 0.05 level. nt, nontransduced.

Abberior635P dye (*SI Appendix*, Fig. S3), S6-$p75^{NTR}$ imaged with total internal reflection fluorescence (TIRF) microscopy appears as a carpet of spots decorating the cell basal membrane,

each corresponding to a single receptor particle (Fig. 2 *A* and *B*). With a Tet-On inducible promoter (24), we tuned receptor expression from low (~0.1 spot per square micrometer) to the highest density allowing us to track p75^{NTR} receptors individually (~0.5 spot per square micrometer), and even to bulk p75^{NTR} expression (Fig. 2*A*). Receptors at densities from 0.1 to 0.45 spot per square micrometer were followed over time (Movies S1 and S2), and tracked at the single-particle level (32) (Fig. 2*B* and Movie S3). We compared wild-type p75^{NTR} (wt p75^{NTR}; Fig. 2*C*) with 2 reference monomeric or dimeric variants of S6-tagged p75^{NTR}. The "monomeric" form contains C256A and G265I mutations on the p75^{NTR} TM domain, which were reported to inhibit covalent and noncovalent receptor dimerization, respectively (17), along with a deletion in its JM region that inhibits intracellular clustering (33) (mutant p75^{NTR} [mut p75^{NTR}]; Fig. 2*C*). The mut p75^{NTR} recapitulated the localization observed for wt p75^{NTR} (*SI Appendix*, Fig. S4 *A* and *B*); importantly, it did not display the high-molecular-weight bands in Western blots (*SI Appendix*, Fig. S4*C*) previously identified as putative receptor oligomeric forms (17, 20). To force dimerization, we replaced the entire wt p75^{NTR} extracellular JM region with the c-jun leucine-zipper domain, as in a study by Brooks et al. (34) (dim p75^{NTR}; Fig. 2*C*).

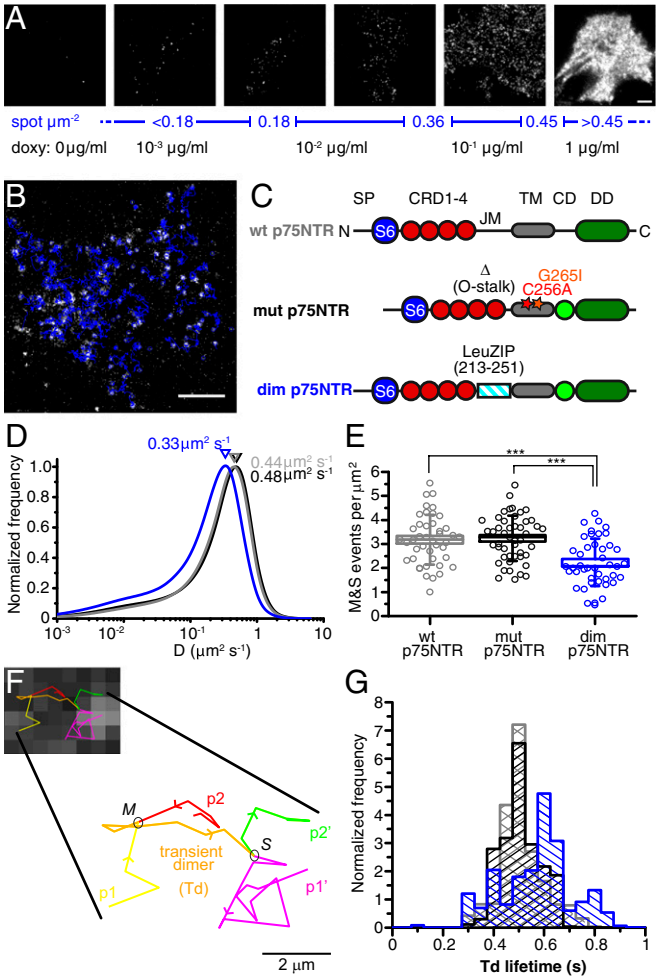

Fig. 2. Membrane dynamics of p75^{NTR} molecules in the cell membrane. (*A*) Expression of S6-p75^{NTR} regulated by doxycycline (doxy). TIRF images of Abberior635P-labeled p75^{NTR} receptors in SK-N-BE(2) cells show the dependence of the number of receptors per area (blue scale) on doxycycline concentration in the medium (black values below). (Scale bar, 5 µm.) (*B*) TIRF image of S6-p75^{NTR} labeled with Abberior635P; superimposed trajectories are shown in blue. (Scale bar, 5 µm.) (*C*) S6-tagged constructs. The wt p75^{NTR} is as in Fig. 1*A*; mut p75^{NTR} bears mutations C256A and G256I, and lacks residues 221 to 246 encompassing the O-stalk domain in the JM region; and dim p75^{NTR} has residues 213 to 251 of the JM portion replaced with the leucine zipper domain (LeuZIP) from c-jun. CD, chopper; DD, death domain; SP, signal peptide. (*D*) Distribution of D for wt p75^{NTR} (gray), mut p75^{NTR} (black), and dim p75^{NTR} (blue). (*E*) Number of M&S events in 500-frame movies, normalized per membrane area, for wt p75^{NTR} (gray), mut p75^{NTR} (black), and dim p75^{NTR} (blue). Boxes represent SE, lines represent median, and whiskers represent SD. ***$P < 0.001$, Kruskal–Wallis test. (*F*) TIRF frame with superimposed transient dimer trajectory, enlarged at the bottom for visualizing the merge (*M*) between p1 (yellow) and p2 (red) particles, their colocalization trajectory (orange) corresponding to a transient dimer (Td), and their split (*S*) in p1′ (magenta) and p2′ (green) particles. (Scale bar, 2 µm.) (*G*) Distribution of the cell-average duration of Td trajectories for wt p75^{NTR} (gray), mut p75^{NTR} (black), and dim p75^{NTR} (blue) constructs. Cells with 0.18 to 0.36 receptor per square micrometer range were considered for these analyses.

In SK-N-BE(2) cells, analysis of the short-time diffusion coefficient (D) distributions, as in studies by Marchetti et al. (21) and Callegari et al. (25), revealed that wt p75^{NTR} and mut p75^{NTR} are indistinguishable, while dim p75^{NTR} is significantly slower, showing a distribution shifted toward D values compatible with what is expected for dimers (35) and a somewhat higher low-D tail (Fig. 2*D*); these data suggest the absence of stable dimers for both wt p75^{NTR} and mut p75^{NTR}. To identify possible transient p75^{NTR} dimers, we analyzed the dynamic association/dissociation of spots during their trajectories (merge and split [M&S] events, shown in Movies S4 and S5 and schematized in Fig. 2*F*), as previously done by Kasai and Kusumi (36). The number of M&S events per membrane area was significantly lower for dim p75^{NTR} than for wt p75^{NTR} and mut p75^{NTR}; the latter 2, instead, did not differ significantly (Fig. 2*E*). This shows that the 3 p75^{NTR} constructs display an observable dynamic equilibrium between monomers and dimers, but while wt p75^{NTR} has association/dissociation kinetics similar to mut p75^{NTR}, dim p75^{NTR} has either a higher dimerization probability or a lower separation rate. We also quantified the mean duration of transient dimerization (Td) events (orange in Fig. 2*F*), i.e., the trajectory segments between a merge event and a split event. The distribution of average Td lifetime demonstrated that while wt p75^{NTR} and mut p75^{NTR} display dimerization events equally peaked between 0.4 and 0.5 s, those of dim p75^{NTR} peak at 0.6 and 0.8 s (Fig. 2*G*). These results allow us to determine that wt p75^{NTR} does not form stable dimers or higher oligomers in the living cell membrane.

Because of the transient nature of p75^{NTR} dimers, as well as of photobleaching during tracking, analysis of the average intensity of the trajectories in live cells could not give an unambiguous answer on the stoichiometry (*SI Appendix*, Fig. S5). Therefore, we analyzed the intensity step photobleaching profile of isolated p75^{NTR}/Abberior635P spots in fixed cells (yellow boxes in Fig. 3*A*). For each spot, we quantified 1) the number of photobleaching steps (red arrows in Fig. 3*B*) and 2) the mean intensity before bleaching (I_{PRE}; green lines in Fig. 3*B*). Both constitute a direct measure of the number of molecules in a spot for receptor membrane oligomerization (37). The vast majority of analyzed wt p75^{NTR} and mut p75^{NTR} spots are monomers; that is, they display 1 photobleaching step (about 77% for both species; Fig. 3*C*). Conversely, the NGF-stimulated S6-TrkA construct displayed a significantly higher proportion of dimers and oligomers (26) (*SI Appendix*, Fig. S6*A*). Importantly, the majority of dim p75^{NTR} spots showed a 2-step photobleaching profile (55%; Fig. 3*C*), and monomers were reduced to 35%. Only dim p75^{NTR} displayed a sizeable amount of spots with 3 and 4 photobleaching steps. I_{PRE} distributions obtained for the 3 p75^{NTR} variants confirmed the bleaching step analysis (*SI Appendix*, Fig. S6*B*).

We underline that some mut p75^{NTR} apparent dimers were detected (about 20% of the analyzed spots) similar to wt p75^{NTR}: This proves the lack of a relationship with the TM residues previously indicated as driving receptor dimerization (17). Overall,

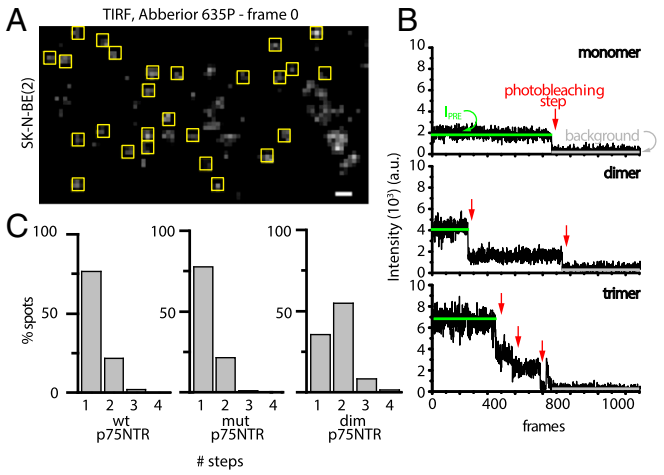

Fig. 3. p75^{NTR} is predominantly a monomer in the cell membrane. (*A*) TIRF image showing receptor spots on the surface of fixed cells (yellow squares represent analyzed spots; analyzed cells had 0.2 to 0.5 spot per square micrometer). (Scale bar, 1 μm.) (*B*) Typical intensity profile traces of a monomer (*Top*), dimer (*Middle*), and trimer (*Bottom*) showing the parameters considered in the calculation. I_{PRE} (green line) is the particle average intensity before the first bleaching step, red arrows point to single photobleaching steps, and the gray line represents background intensity. a.u., arbitrary units. (*C*) Photobleaching steps per trace for wt p75^{NTR}, mut p75^{NTR}, and dim p75^{NTR}.

our experiments distinguish between the diffusivity of monomers and dimers, and challenge the existence of stable p75^{NTR} dimers in the membrane of live cells.

wt p75^{NTR} and mut p75^{NTR} Display Different Membrane Partitioning in Response to NGF Stimulation. We next compared wt p75^{NTR} and mut p75^{NTR} membrane diffusivity following NT stimulation, to see if this might impact the oligomeric state of the receptor. Also, we aimed at identifying a possible molecular basis, an alternative to the lack of oligomerization, as the source of the impaired apoptotic signaling of mut p75^{NTR} following NT stimulation (17, 18).

We measured D values from trajectories of wt p75^{NTR} and mut p75^{NTR} with or without 15 min of NGF stimulation. The diffusivity of both constructs upon NGF treatment remained significantly higher than that of the dim p75^{NTR} construct (Fig. 4*A*). This suggests that NGF does not induce dimerization of either construct. These data are consistent with the absence of fluorescence resonance energy transfer (FRET) or homo-FRET changes following NT addition in cells expressing fluorescent p75^{NTR} constructs (17, 38). However, NGF elicits a small but statistically significant shift of D distributions of the 2 constructs in opposite directions (i.e., it slightly slows down wt p75^{NTR}, while it speeds up mut p75^{NTR}). Similarly, a slowing down of wt p75^{NTR} was observed in proNGF-treated neurons (*SI Appendix*, Fig. S7). Since these changes are not compatible with gain or loss of stable oligomerization, we reasoned that they might stem from wt p75^{NTR} and mut p75^{NTR} movements across membrane areas with different composition. In this scenario, lipid rafts may represent the discriminating factor, as they could confine and alter transiently the diffusivity of membrane proteins (39). Cholesterol plays a key structural role in lipid rafts, and the association of proteins with lipid rafts can be detected experimentally by testing cholesterol-dependent, confined diffusion (40). Consistently with this, p75^{NTR} mobility was found to depend on the cholesterol content in the plasma membrane (41), and we measured a clear anticorrelation between its D value and membrane cholesterol in 6 cellular models (Fig. 4*B* and *SI Appendix*, Fig. S8). The fastest p75^{NTR} diffusivity is observed in cortical neurons, which display the lowest membrane cholesterol levels of our survey; SK-N-BE(2) cells have a cholesterol content similar to neurons, thus validating the choice of this model system to study p75^{NTR} membrane dynamics.

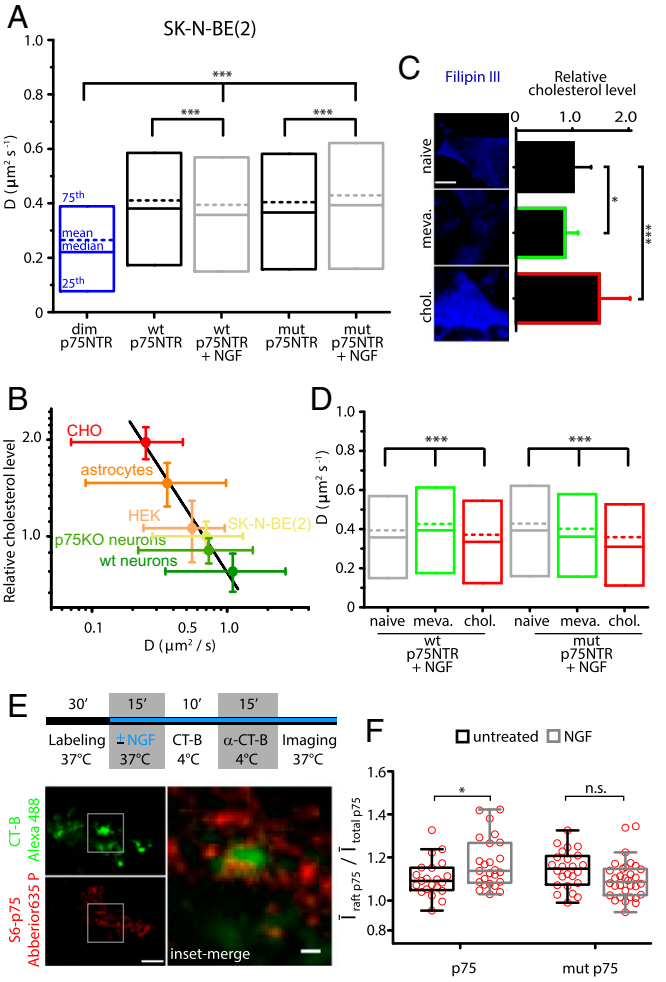

Fig. 4. Membrane cholesterol regulates p75^{NTR} diffusivity and response to NGF. (*A*) Box-plot for D values from trajectories of wt p75^{NTR} or mut p75^{NTR} in SK-N-BE(2) cells in resting conditions (black) and up to 15 min after NGF administration (gray); the distribution for dim p75^{NTR} (blue) is also shown. Boxes represent 25th to 75th percentiles, lines represent medians, and dashed lines represent means. ***$P < 0.001$, Kruskal–Wallis test (with Dunn's means comparison). (*B*) Plot of membrane cholesterol (CHO) content (mean intensity ± SEM of filipin III-stained cells) versus D of p75^{NTR} single molecules (peak ± full width at half maximum of its distribution as in *SI Appendix*, Fig. S8*C*) in 6 different cell models. Cholesterol content is normalized to SK-N-BE(2) cell results. The black line indicates linear fit. HEK, human embryonic kidney 293 cells. (*C*) TIRF images of filipin III-stained SK-N-BE(2) cells exhibiting modulation of cholesterol levels (quantified as mean intensity ± SEM) with mevastatin (meva., green) or soluble cholesterol (chol., red). *$P <$ 0.05 and ***$P < 0.001$, 1-way ANOVA. (Scale bar, 10 μm.) (*D*) Same graph as in *A*, obtained for NGF-stimulated wt and mut S6-p75^{NTR} trajectories in SK-N-BE(2) cells (gray), treated with mevastatin (green) and cholesterol (red). ***$P < 0.001$, Kruskal–Wallis test (with Dunn's means comparison). (*E*) Outline of the colocalization experiment with TIRF images of cholera toxin B subunit (CT-B)-stained GM1 (green) and p75^{NTR} single molecules (red). (Scale bar, 5 μm; *Inset*, 1 μm.) (*F*) Quantification of wt/mut p75^{NTR} and CT-B colocalization in the absence or presence of NGF. Box-plots show median and 25th to 75th percentiles of average p75^{NTR} intensity inside CT-B–stained domains ($\bar{I}_{raft\ p75}$) over average p75^{NTR} intensity within the whole cell ($\bar{I}_{total\ p75}$). Whiskers indicate Tukey intervals, and red circles represent individual data. *$P = 0.016$, 1-way ANOVA (with Bonferroni comparison of means). ns, not significant at the 0.05 level.

Given that raft domains are crucial for apoptotic signaling via $p75^{NTR}$ (42), we considered that differential residency of wt $p75^{NTR}$ and mut $p75^{NTR}$ upon NT binding in these areas might explain not only the D changes observed (Fig. 4*A*) but also their different signaling abilities. To test this hypothesis, we first monitored NGF-driven diffusivity of the 2 receptor forms following up- or down-regulation of membrane cholesterol in SK-N-BE(2) cells (Fig. 4*C*). While increasing membrane cholesterol slows down both receptor forms, removal of membrane cholesterol has 2 opposite outcomes: wt $p75^{NTR}$ is accelerated, while mut $p75^{NTR}$ slowed (Fig. 4*D*). Since the effect of cholesterol depletion on lateral diffusion depends on the composition of the membrane regions explored by the membrane receptors (43), these data suggest that wt $p75^{NTR}$ and mut $p75^{NTR}$ partition into different membrane areas after NGF binding. These relocalizations most probably occur in a very dynamic way, given the small diffusivity changes involved (Fig. 4*A* and *SI Appendix*, Fig. S7). Indeed, biochemical isolation of raft domains showed wt $p75^{NTR}$ localizing in both raft and nonraft regions, in the absence and presence of NGF (44, 45). Thus, to capture transient raft occupancy, we imaged lipid rafts and $p75^{NTR}$ simultaneously, after 15 min of NGF stimulation, by dual-color TIRF microscopy (Fig. 4*E*), similar to the method used by Pinaud et al (46). Rafts were visualized by cross-linking membrane ganglioside GM1 with a fluorescent cholera toxin B subunit (47). NGF stimulation significantly increases the localization of wt $p75^{NTR}$ in GM1 regions, but not that of mut $p75^{NTR}$ (Fig. 4*F*).

We conclude that $p75^{NTR}$ translocates to lipid rafts upon NGF binding, and mut $p75^{NTR}$ has a reduced residency in cholesterol-rich membrane microdomains upon NGF binding compared with the wt counterpart. Notably, in the absence of competing Trk receptors, both NTs and proNTs induce coherent effects on $p75^{NTR}$ in terms of both membrane diffusivity (Fig. 4*A* and *SI Appendix*, Fig. S7) and biological activity; for instance, proBDNF induces apoptosis via $p75^{NTR}$ (18), but $p75^{NTR}$ also mediates apoptosis in retinal neurons by NGF (48) and in sympathetic neurons by BDNF (49).

Membrane Cholesterol Regulates $p75^{NTR}$ Apoptotic Signaling. Following previous observations, we tested if membrane cholesterol levels also affected NT-dependent apoptotic signaling via $p75^{NTR}$; here, C256 TM residue was shown to play a crucial role (17, 18). Treating neurons with mevastatin and methyl-beta-cyclodextrin (MβCD) strongly decreases membrane cholesterol, as measured by filipin staining, while loading neurons with cholesterol has the opposite effect (Fig. 5 *A* and *B*). The proBDNF-induced apoptosis was abolished in cholesterol-depleted cortical neurons from wt mice, while it was slightly increased upon cholesterol overload (Fig. 5*C*). Cholesterol modulation was also applied to wt $p75^{NTR}$ and mut $p75^{NTR}$ (Fig. 5 *D*–*F*) transduced in $p75^{NTR}$ KO mouse neurons and induced with 0.05 μg/mL doxycycline, a concentration not leading to overexpression (Fig. 2*A*). The $p75^{NTR}$ KO neurons were not responsive to proBDNF; wt $p75^{NTR}$, but not mut $p75^{NTR}$, restored proapoptotic signaling (Fig. 5*D*). When neurons were treated with mevastatin/MβCD, wt $p75^{NTR}$ lost its ability to induce apoptosis, confirming our results on wt neurons (Fig. 5 *C* and *E*). Conversely, cholesterol administration boosted proapoptotic signaling of wt $p75^{NTR}$ (Fig. 5 *F* and *G*); surprisingly, the same treatment also conferred apoptotic capability to mut $p75^{NTR}$ (Fig. 5 *F* and *G*). This was not an effect of the combination of proBDNF and cholesterol load: Untransduced neurons from $p75^{NTR}$ KO mice were not responsive in these conditions (Fig. 5*F*).

From these results, we conclude that the inability of mut $p75^{NTR}$ to induce apoptosis (18) (Fig. 5*D*) is due to its poorer occupancy of cholesterol-rich membrane regions when compared with wt $p75^{NTR}$, rather than to impaired signaling of the protein per se. Accordingly, under membrane-saturating conditions obtained inducing $p75^{NTR}$ expression with 1 μg/mL doxycycline (Fig. 2*A*), both mut $p75^{NTR}$ and wt $p75^{NTR}$ were able to induce apoptosis (*SI Appendix*, Fig. S9). These findings, along with those obtained in SK-N-BE(2) cells (Fig. 4), show that NT binding regulates the partitioning of $p75^{NTR}$ in and out of lipid rafts, thereby regulating its ability to induce apoptosis.

Surface-Exposed $p75^{NTR}$ Mediates Growth Cone Collapse in the Presence and Absence of proNGF. Growth cone retraction caused by overexpression of both wt $p75^{NTR}$ and a C256A $p75^{NTR}$ mutant was reported to occur upon proNGF administration in developing neurons (20). Hence, $p75^{NTR}$ collapse action may not necessarily depend on receptor partitioning in cholesterol-rich regions, unlike apoptotic signaling (Fig. 5). We therefore investigated the mechanisms of axonal growth regulation by $p75^{NTR}$. We found that endogenous levels of $p75^{NTR}$ can also regulate axon branching. Axonal arbors of CA3 neurons projecting into the CA1 region are significantly more ramified and occupy larger areas in $p75^{NTR}$ KO mice than in wt mice (*SI Appendix*, Fig. S10 *A* and *B*). This is reflected in a higher number of synaptic boutons (*SI Appendix*, Fig. S10*C*), consistent with previous observations of $p75^{NTR}$ KO animals showing increased dendritic complexity (50). Neuronal cultures of the same animals recapitulated this result (Fig. 6 *A* and *B*), with $p75^{NTR}$ KO axons being longer (Fig. 6*C*) and displaying an increased number of branch points (Fig. 6*D*) and lateral growth cones per length unit (Fig. 6*E*) with respect to wt axons. Importantly, transient expression of wt $p75^{NTR}$ or mut $p75^{NTR}$ constructs in $p75^{NTR}$ KO neurons completely rescued the phenotype observed in wt neurons (Fig. 6 *C*–*E*). In agreement with previous data (20), expression of either wt $p75^{NTR}$ or mut $p75^{NTR}$ in hippocampal neurons leads to growth cone collapse in response to proNGF (*SI Appendix*, Fig. S11 *A* and *B*). Overall, this suggests that the regulation of axonal complexity and proNT-dependent collapse of growth cones share a common mechanism regulated by $p75^{NTR}$ independently on Cys256 and other residues mutated or missing in mut $p75^{NTR}$ (Fig. 2*C*).

To gain further insight into this mechanism, we monitored the membrane pool of S6-$p75^{NTR}$–EGFP during collapse by biotinylating the receptors on the cell surface before proNGF incubation, and detecting receptors still present on the plasma membrane with streptavidin-Qdot after proNGF incubation for 30 min; EGFP fluorescence marked the total content of $p75^{NTR}$ (Fig. 7*A*). The proNGF caused a dramatic increase in the membrane pool of both wt $p75^{NTR}$ and mut $p75^{NTR}$, while lower levels of membrane $p75^{NTR}$ were detected in untreated neurons (Fig. 7 *B* and *C*). Inhibition of dynamin-dependent internalization with Dynasore (Fig. 7*D*), to maintain wt and mut S6-$p75^{NTR}$–EGFP on the surface regardless of proNGF administration (Fig. 7*E*), was sufficient to drive the growth cone collapse, independently from ligands; indeed, proNGF had no further collapse-inducing effect, implying that $p75^{NTR}$ exposure is a downstream event to ligand binding (Fig. 7*F* and *SI Appendix*, Fig. S11*A*). Notably, Dynasore alone in untransfected neurons did not have such a prominent effect, although a trend could be observed upon drug treatment and proNGF administration (Fig. 7*F*); this is likely due to a fraction of hippocampal neurons expressing detectable levels of $p75^{NTR}$, as previously shown (29). Inhibiting $p75^{NTR}$ internalization by expressing the K44A dominant negative form of dynamin had the same effect (*SI Appendix*, Fig. S11 *D* and *E*), confirming the results obtained with Dynasore. Furthermore, we found that the mechanism responsible for the removal of $p75^{NTR}$ from the plasma membrane in the absence of proNGF is dependent on clathrin, as blocking clathrin-dependent endocytosis by Pitstop2 was sufficient to accumulate surface $p75^{NTR}$ and trigger neuronal growth cone collapse (Fig. 7 *G*–*J*).

These data suggest that $p75^{NTR}$ has an intrinsic collapsing activity when retained on the growth cone membrane, and internalization inhibition is a sufficient driving force that does not

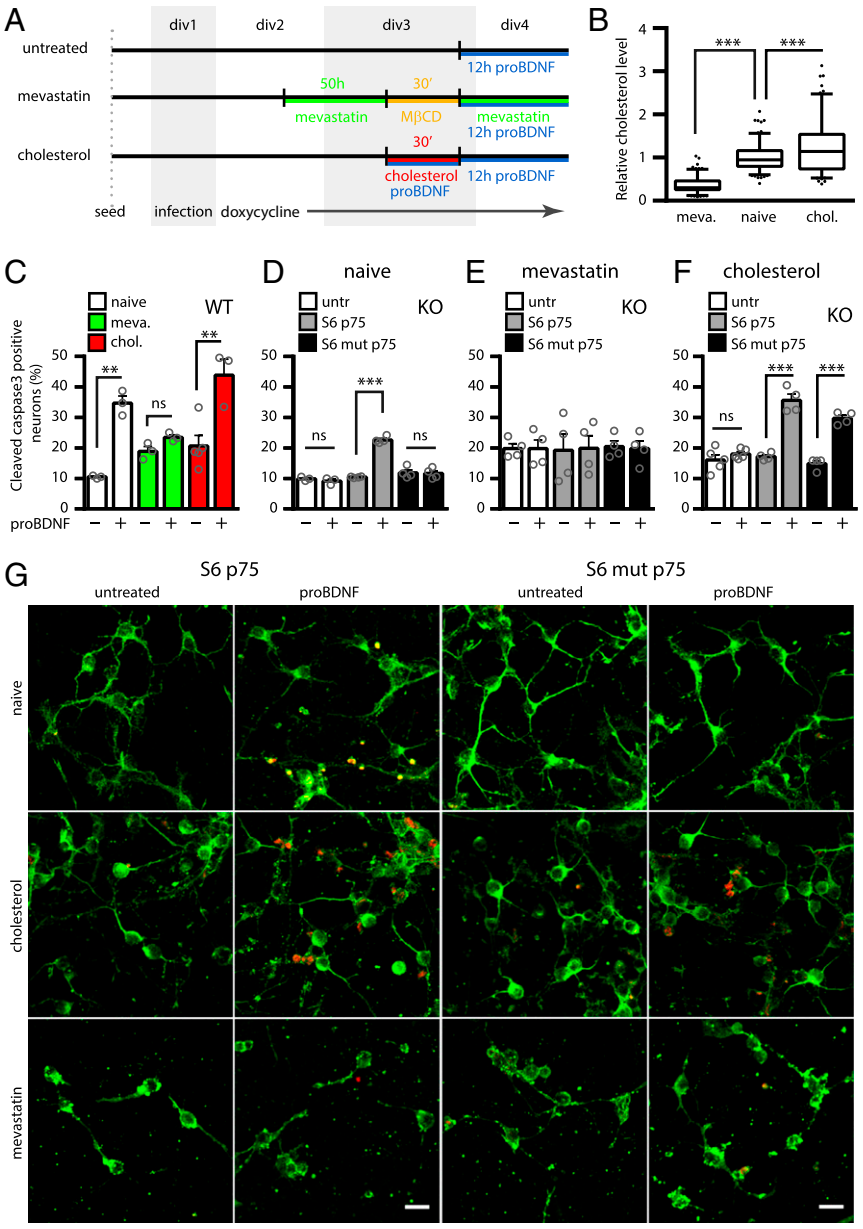

Fig. 5. Membrane cholesterol regulates proBDNF apoptotic signaling via $p75^{NTR}$. Experimental timeline (*A*) and quantification of cholesterol (intensity of filipin III staining) in cortical neurons treated with mevastatin/MβCD (meva.) or soluble cholesterol (chol.), relative to untreated neurons (*B*). ***$P < 0.001$, 1-way ANOVA (Tukey's multiple comparisons). Box-plots represent 25th to 75th percentiles, whiskers indicate Tukey intervals, and dots represent outliers. div, day in vitro. (*C*) Percentage of cleaved caspase-3–positive neurons in wt cortical neurons (naive, white columns) or in the same neurons treated with mevastatin (green columns) or cholesterol load (red columns) in the absence or presence of proBDNF. (*D*) Percentage of cleaved caspase-3–positive neurons in untransduced $p75^{NTR}$ KO cortical neurons (untr [untransduced], white columns) or in the same neurons transduced with wt $p75^{NTR}$ (gray columns) or mut $p75^{NTR}$ (black columns) and induced with 0.05 μg/mL doxycycline, with or without proBDNF. White and gray columns are reported from Fig. 1*F*. The same is shown in conditions of cholesterol depletion (*E*, mevastatin) and cholesterol load (*F*, cholesterol) of the neurons. For *C*–*F*, **$P < 0.01$ and ***$P < 0.001$, 1-way ANOVA test (with Tukey's comparison of means). ns, not significant at the 0.05 level. Bars are mean ± SEM, and superimposed dots represent samples. (*G*) Representative confocal images of neurons expressing wt $p75^{NTR}$ or mut $p75^{NTR}$, untreated or treated with proBDNF. Naive neurons (*Top*), cholesterol-enriched (cholesterol) neurons (*Middle*), and cholesterol-depleted (mevastatin) neurons (*Bottom*) are shown. MAP2 (green) and cleaved caspase-3 (red) are indicated. (Scale bars, 20 μm.)

necessarily require NT-induced partitioning into raft domains. Indeed, both wt $p75^{NTR}$ and mut $p75^{NTR}$ constructs similarly regulate axonal complexity. Overexpression has been called into question in the evaluation of growth cone collapse (18). Indeed, $p75^{NTR}$ expression by a constitutively strong promoter results in a many-fold expression increase compared with that of $p75^{NTR}$ induced at 0.05 μg/mL doxycycline (*SI Appendix*, Fig. S12), which recapitulates the behavior of endogenous $p75^{NTR}$ (Fig. 5). We therefore evaluated the effect of proNGF on neurons infected with wt $p75^{NTR}$ or mut $p75^{NTR}$ and induced with 0.05 μg/mL or 1 μg/mL doxycycline (*SI Appendix*, Fig. S13*A*). We found that growth cone collapse could still be observed, although at lower levels than with overexpressed $p75^{NTR}$. The growth cone area decreases with increasing surface $p75^{NTR}$ density: In particular, a threshold for growth cone collapse was found in the range of 1 to 2 receptors per square micrometer (*SI Appendix*, Fig. S13 *B* and *C*). Although slightly higher than the receptor ranges explored in our advanced imaging (Fig. 3 and *SI Appendix*, Fig. S7) and apoptosis assays (Fig.

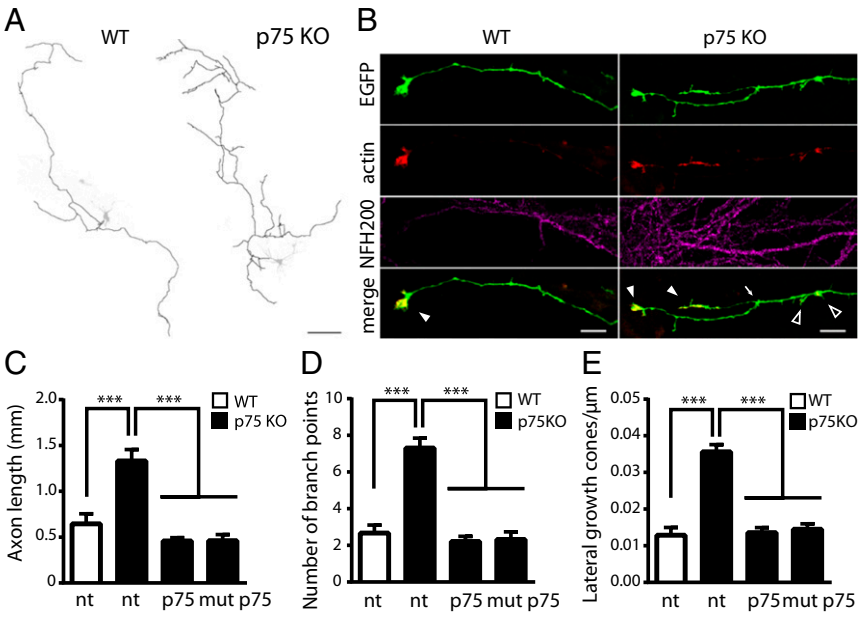

Fig. 6. wt p75^{NTR} and mut p75^{NTR} mediate growth cone collapse and regulate axon complexity. (*A*) Hippocampal neurons from wt (*Left*) and p75^{NTR} KO (*Right*) mice. Axons from EGFP- and TagRFP-actin–expressing neurons are drawn in black and superimposed to the EGFP channel (grayscale). (Scale bar, 100 µm.) (*B*) Magnification of axon terminals from images in *A* also showing immunofluorescence for the axonal marker NF-200. TagRFP-actin accumulates at growth cones. Branching points (arrow), terminal growth cones (filled arrowheads), and lateral growth cones (empty arrowheads) are indicated. (Scale bars, 5 µm.) Quantification of axon length (*C*), number of branch points (*D*), and number of lateral growth cones per length unit (*E*) are illustrated in non-transfected (nt) wt hippocampal neurons (white columns), in nt p75^{NTR} KO hippocampal neurons (black columns), or transfected with wt p75^{NTR} or mut p75^{NTR} constructs (wt/mut p75^{NTR}, black columns). ***$P < 0.001$, Kruskal–Wallis test (Dunn's multiple comparisons). Bars are mean ± SEM.

5), this value seems compatible with physiological levels observed at least in a subset of central neurons displaying sufficient p75^{NTR} levels to drive cone retraction (29). At 0.05 µg/mL doxycycline, p75^{NTR} explores a range of expression levels on the neuronal surface, with densities spanning from below to above the range of 1 to 2 receptors per square micrometer, and this explains why only a subpopulation of neurons undergoes growth cone collapse in this sample (*SI Appendix*, Fig. S13). Importantly, the growth cone area distribution for mut p75^{NTR} neurons was not significantly different from that for wt p75^{NTR}, and the 2 forms displayed similar area versus p75^{NTR} level dependency (*SI Appendix*, Fig. S13*C*), thus ruling out overexpression as the cause for their identical behavior (Fig. 6). This demonstrates that growth cone collapse via p75^{NTR} can occur at receptor levels close to or slightly higher than the natural average density in neurons, and that both p75^{NTR} forms are equally capable of mediating it.

Discussion

To solve the oligomerization conundrum of p75^{NTR} in a live cell context and to gain insight into its mechanisms of activation by NTs, we applied a single-molecule fluorescence approach that we had already validated to image and track NT receptors and their ligands (21–25). This avoids the use of indirect methods like labeled antibodies or ligands and obviates the problem of Qdot steric hindrance (51) (*SI Appendix*, Fig. S3). In neuroblastoma cells (Movie S1 and Figs. 2*D* and 4*A*), as well as in primary neurons (Fig. 4*B*, *SI Appendix*, Fig. S7, and Movie S2), p75^{NTR} exhibits fast dynamics and is mostly present in monomeric form. NT or proNT stimulations do not alter its stoichiometry significantly (Figs. 3 and 4*A*); instead, our data show that p75^{NTR} molecules only form transient homointeractions if any (Figs. 2 *E*–*G* and 3), indicating that dynamic interactions are likely to underlie receptor activation.

The existence of preformed p75^{NTR} oligomers in the membrane has been hotly debated, with different groups reporting p75^{NTR} dimers (1, 17), trimers (13), or a mixture of both (16, 20). Evidence for oligomerization mostly came from the electrophoretic shift of the immunodetected receptor band of 2- or 3-fold the weight of the monomer, in nonreducing conditions or after chemical cross-linking. However, this constitutes an indirect way of investigating stoichiometry. Indeed, both run length and intensity of higher weight bands in a gel critically depend on several technical parameters, such as lysis conditions, antibody, or composition of the gel (*SI Appendix*, Table S1 and compare, e.g., *SI Appendix*, Figs. S4 and S14). Heavier p75^{NTR}-immunoreactive bands may be the result of p75^{NTR} homo- or hetero-aggregation with unknown proteins or lipids in close proximity. Indeed, p75^{NTR} association with gangliosides in response to ligands was already reported (52). Thus, the shifted bands could simply reflect crowding of molecules interacting transiently in cholesterol-rich regions, which are stabilized by certain lysis conditions, rather than a stable physical association. This is supported by the recent observation that the putative oligomeric shifted band of another TNF receptor, Death Receptor 5, is impaired by cholesterol-depletion treatments (53). Here, we provide a direct and quantitative estimate of the human full-length p75^{NTR} oligomerization state in the cell membrane. Our data on dynamics and bleaching steps demonstrate a predominant monomeric p75^{NTR} form (~77%; Fig. 3*B*). Notably, this percentage is almost identical (Fig. 3*B*), as is the diffusive profile (Fig. 2 *D*–*G*), to a reference monomeric p75^{NTR} construct (mut p75^{NTR}), which bears all mutations impairing p75^{NTR} gel-shifted bands (17, 20, 33) (Fig. 2*C*). Therefore, even if ~22% of p75^{NTR} apparent dimers are detected, they are not dependent on the mutated or deleted residues; this fraction likely constitutes an overestimation due to nonresolved pairs of individual monomers merely in proximity, especially in small zones on the membrane where diffusivity is hindered; a similar effect could also explain the presence of trimers and tetramers for dim p75^{NTR}. For G protein-coupled receptors, apparent oligomers

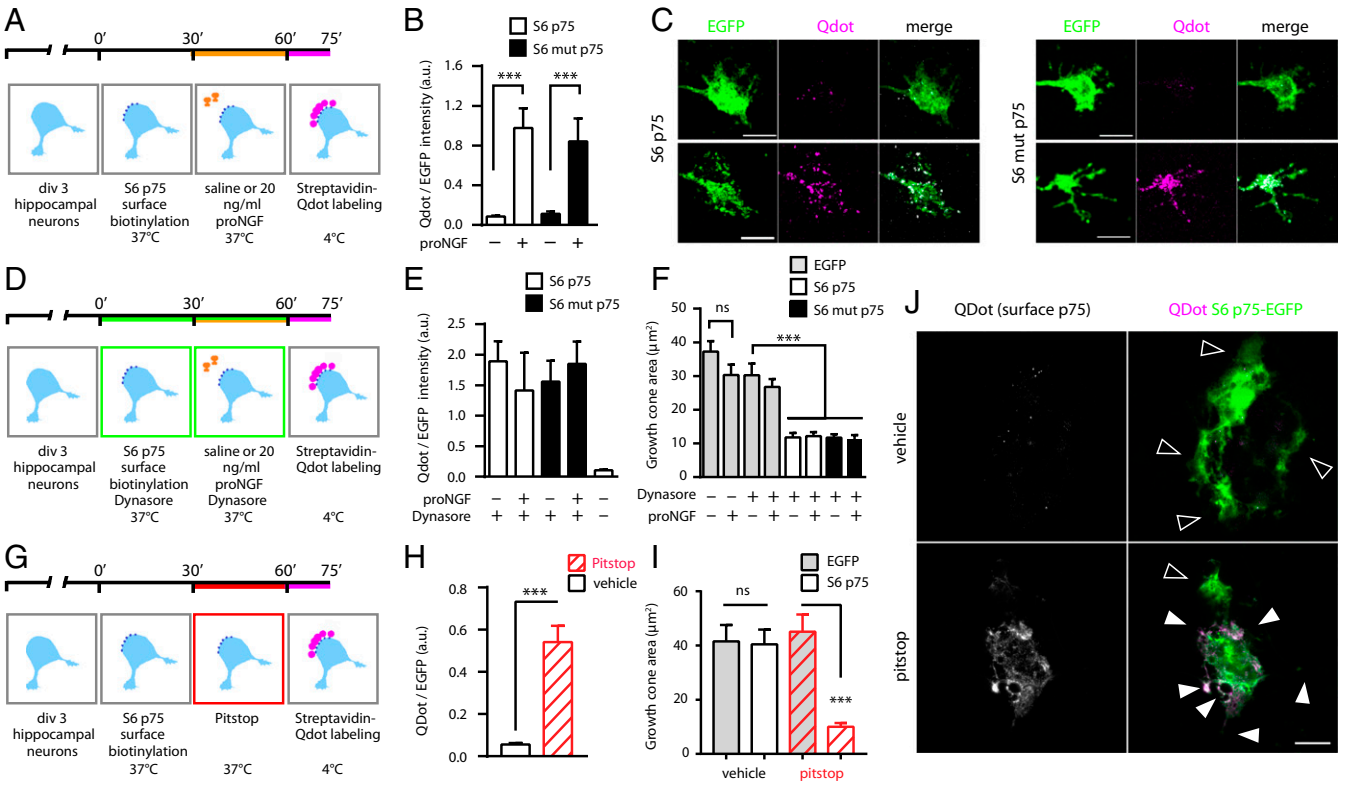

Fig. 7. Surface-exposed p75^{NTR} mediates growth cone collapse in the presence and absence of proNGF. (*A*) Timeline of the experiment to detect surface S6-p75^{NTR}–GFP after proNGF administration. (*B*) Qdot-to-EGFP ratio is a measure of surface p75^{NTR}-EGFP. Both wt p75^{NTR} and mut p75^{NTR} are enriched on the plasma membrane after 30 min of proNGF treatment. ***$P < 0.001$, Kruskal–Wallis test (Dunn's multiple comparisons). Bars are mean ± SEM. a.u., arbitrary units. (*C*) Confocal images of growth cones of wt hippocampal neurons, transfected with S6-tagged wt p75^{NTR}-EGFP (*Left*) and mut p75^{NTR}-EGFP (*Right*) constructs, untreated (*Top*) or treated with proNGF for 30 min (*Bottom*). Total (green) and surface (magenta) receptor pools are shown, and are quantified in *B*. EGFP channel levels have been linearly scaled to highlight cone dimensions. (Scale bars, 5 μm.) (*D*) Timeline of the experiment with Dynasore internalization-inhibiting drug. (*E*) Dynasore increases the Qdot-to-EGFP ratio even without proNGF, confirming the retention of wt and mut p75^{NTR}-EGFP on the plasma membrane. (*F*) Retention on the membrane is sufficient for wt p75^{NTR} and mut p75^{NTR} to cause growth cone collapse. Corresponding images are shown in *SI Appendix*, Fig. S11*A*. ***$P < 0.001$, 1-way ANOVA (Tukey's multiple comparisons). ns, not significant at the 0.05 level. Bars are mean ± SEM. (*G*) Experimental timeline with Pitstop2 internalization-inhibiting drug. (*H*) Inhibiting clathrin-dependent internalization causes accumulation of surface p75^{NTR}. ***$P < 0.001$, Welch's test (2-tailed). (*I*) Retention of p75^{NTR} is sufficient to cause growth collapse without proNGF. ***$P < 0.001$, 1-way ANOVA (Bonferroni multiple comparisons). Bars are mean ± SEM. (*J*) Representative neurons expressing S6-p75^{NTR}–EGFP treated with Pitstop2 or vehicle. Highlighted are extended (empty arrowheads) and collapsed (filled arrowheads) growth cones. Collapsed growth cones show increased surface p75^{NTR} levels, suggesting a cone-autonomous mechanism. (Scale bar, 10 μm.)

were quantified to be a 3/6-fold overestimation in similar ranges of receptor densities (54).

Our dynamics data question the possibility of a covalent TM p75^{NTR} dimerization, challenging a previous model for the p75^{NTR} mechanism of action, which postulates that NT binding to the putative preformed p75^{NTR} covalent dimer induces a conformational change propagated via Cys256, leading to separation of death domains (17). This model was already challenged by structural considerations on the flexibility of the JM and chopper domains (19). We propose an alternative molecular basis for receptor activation, in which p75^{NTR} monomers preferentially concentrate into signaling-competent membrane microdomains, like lipid rafts, upon NGF stimulation, with C256 and G265 residues playing a crucial role in this compartmentalization (Fig. 8*A*). Indeed, the importance of Cys256 was corroborated by the failure of proBDNF-induced neuronal apoptosis in mut p75^{NTR} knock-in mice (18). This is supported by the observation that wt (but not mut) p75^{NTR} displays higher average residency in GM-1–rich regions upon NGF binding (Fig. 4 *E* and *F*), and that the diffusion of NGF-bound wt p75^{NTR} and mut p75^{NTR} displays different responses to cholesterol-modulation treatments (Fig. 4*D*).

Robust evidence correlates NT signaling, especially proapoptotic signaling, to the residency of NT receptors in lipid rafts, probably because many interactors and effectors of the pathway are commonly associated with these regions (42, 44, 55). Indeed, p75^{NTR} palmitoylation (Fig. 1*C*) can mediate the association of the protein with lipid rafts (1), and is necessary for p75^{NTR} proapoptotic activity (27). Hence, p75^{NTR} may be capable of activating apoptosis in these zones only, and lack of proBDNF-induced apoptosis by mut p75^{NTR} (Fig. 5*D*) can be explained by its inability to enter these regions upon NT binding (Fig. 8*A*). Our diffusivity data with cholesterol modulation also point to this interpretation (Fig. 4 *C*–*F*). It is unclear to us why the modifications of TM residues may impair the residency of p75^{NTR} in lipid rafts. Available models (38) and NMR structures (56) of the p75^{NTR} TM domain agree in not mapping the 2 residues on the same side of the TM helix. We speculate that these residues are involved in creating peculiar interfaces that bind specific lipids (possibly cholesterol itself) or proteic components of lipid rafts; in support of this, cholesterol depletion impaired proBDNF-induced apoptosis (Fig. 5*E*).

Despite their difference in apoptotic signaling, wt p75^{NTR} and mut p75^{NTR} are equally capable of mediating growth cone collapse in developing neurons (20) (*SI Appendix*, Fig. S11 *A* and *B*). Here, we showed that this effect is linked to the local concentration of the receptor on the growth cone surface. Although it was previously evaluated in p75^{NTR} overexpression regimes

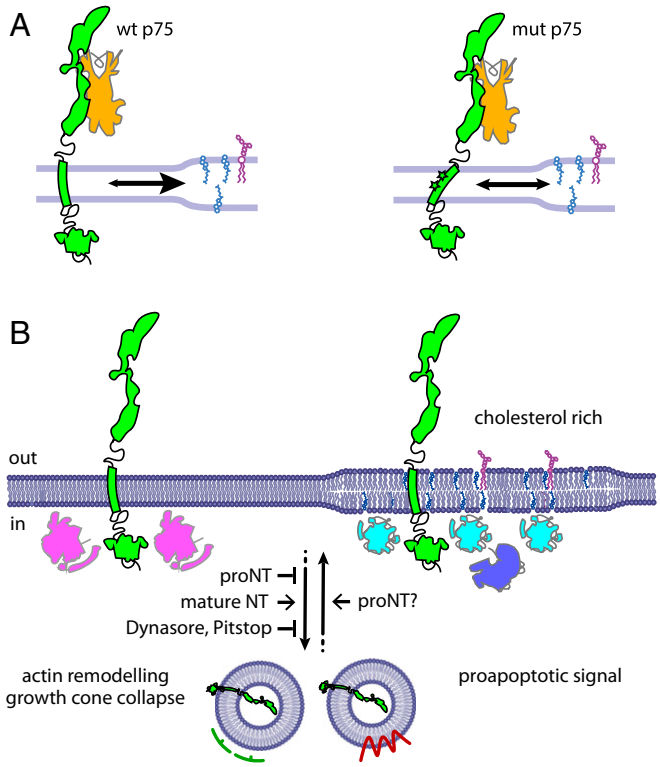

Fig. 8. Proposed model for p75^{NTR} signaling on the plasma membrane. (*A*) Model of the membrane partitioning undergone by wt p75^{NTR} (*Left*, green) or mut p75^{NTR} (*Right*, green) upon NGF (orange) binding. Cholesterol-rich, signaling-competent regions are represented with increased membrane thickness and containing cholesterol and gangliosides. Partitioning is highlighted by the arrows in opposite directions. (*B*) Model of p75^{NTR} signaling at the membrane and downstream internalization. Signaling can occur from cholesterol-poor or cholesterol-rich membrane regions, resulting in receptor internalization within clathrin-positive (green) or caveolin-positive (red) endosomes. In our model, interactors of surface-retained p75^{NTR} (magenta), involved in actin remodeling and growth cone collapse, are more abundant in nonraft regions as this pathway is not impaired by the mutations introduced in mut p75^{NTR}. Conversely, apoptotic signaling effectors (light and dark blue) are enriched in raft platforms being efficiently activated only by NGF-bound wt p75^{NTR}. Different from mature NTs, proNTs at the growth cones cause surface accumulation of p75^{NTR}, which could arise from internalization inhibition (as for Dynasore and Pitstop2 treatments or expression of the dominant negative K44A dynamin) or by increased receptor recycling at the membrane.

(20, 29), we show here that it is still observed when p75^{NTR} is ∼4- to 20-fold less expressed (*SI Appendix*, Fig. S12), thus falling in a range of concentrations compatible with the endogenous levels (*SI Appendix*, Fig. S13). This is particularly plausible if the observed polarized distribution of surface p75^{NTR} is taken into account (Fig. 1*D*). The mechanism is likely to support collapse in a cone-autonomous way. Indeed, collapsed cones show higher levels of surface p75^{NTR} than extended ones even within the same neuron (Fig. 7*J*). The p75^{NTR} surface density is most probably controlled by removal from the plasma membrane and sequestration in intracellular stores. Acute proNGF administration increases both wt p75^{NTR} and mut p75^{NTR} surface pools at growth cones, and inhibition of p75^{NTR} internalization mimics the proNT effect (Fig. 7 and *SI Appendix*, Fig. S11). Although we cannot tell whether proNGF prevents p75^{NTR} internalization or increases p75^{NTR} recycling onto the plasma membrane (Fig. 8*B*), we argue that a signaling cascade activated by surface-exposed p75^{NTR} is responsible for growth cone retraction and axonal complexity. This mechanism could be activated by proNT binding, p75^{NTR} local accumulation (28), or interactions with membrane partners like ephrin-A (57), eventually leading to Rac and RhoA activation (29, 58). It is also possible that p75^{NTR} binds different proteins on the plasma membrane and intracellular stores, possibly regulating their availability. In any case, this activity is not dependent on the TM and JM residues mutated or missing in mut p75^{NTR}, and therefore on the membrane partitioning necessary for proapoptotic signaling (Fig. 8). Accordingly, axonal extension and branching are enhanced in p75^{NTR} KO hippocampal neurons (Fig. 6 *A* and *B* and *SI Appendix*, Fig. S10) and this enhancement is suppressed by either wt p75^{NTR} or mut p75^{NTR} expression (Fig. 6 *C*–*E*). These data corroborate the observation that sympathetic sprouting is enhanced in p75^{NTR}-exIII and p75^{NTR}-exIV KO mice (59). In addition, p75^{NTR}-exIII and p75^{NTR}-exIV KO neurons display increased dendritic complexity, and p75^{NTR}-rich dendritic regions are particularly devoid of collateral branches (50).

In summary, our results demonstrate that p75^{NTR} exists predominantly as a fast-diffusing monomer at the neuronal plasma membrane, and that its signaling capabilities depend on the membrane microdomains traversed and on the amount of surface-exposed receptor available in particular neuronal compartments. Interestingly, while this paper was in preparation, the existence of TrkB dimers was challenged by demonstrating that this receptor is mostly active as monomer on the plasma membrane: This posed severe doubts regarding a long-accepted view of TrkB dimerization as a key step in the transduction of BDNF signaling, partially supported by electrophoretic shifts after chemical cross-linking (60). A scenario emerges in which availability of NT receptor monomers is a fundamental step for signal transduction via Trk-NT-p75^{NTR} constructs induced by the binding of clustered forms of NTs, as recently proposed based on structural data (61). It remains to be established, however, whether coexpression of Trks results in changes of the p75^{NTR} oligomerization state in the cell plasma membrane. In any case, the multifaceted mechanisms of action of the p75^{NTR} monomer suggested by our findings can successfully reconcile most of the apparently conflicting data reported in the literature for the structure and function of this pleiotropic receptor.

Material and Methods

Stoichiometry by Single-Molecule Step Photobleaching. The wt p75^{NTR}, mut p75^{NTR}, and dim p75^{NTR} constructs were transduced in SK-N-BE(2) cells, labeled with Abberior 635P and then fixed for 90 min at room temperature with 4% paraformaldehyde, 5% sucrose, and 0.1% glutaraldehyde in phosphate-buffered saline (PBS); washed 5 times with PBS; and imaged in PBS on the TIRF microscope. Three thousand-frame movies were acquired in a 32.68 × 32.68-μm region of interest centered on the selected cells, with 21 ms of integration time. Time series were then analyzed as described previously (37).

Cleaved Caspase-3 Assay. Cortical neurons from wt p75^{NTR} and p75^{NTR} KO mice seeded on coverslips were left untreated or transduced with wt/mut p75^{NTR}. On day in vitro 3 (DIV3), neurons were treated for 12 h with 20 ng/mL human proBDNF. Samples were then fixed in cold 1:1 acetone/methanol solution for 15 min at −20 °C and processed for immunofluorescence with anti–cleaved caspase-3 (1:300, 9664; Cell Signaling Technology) and anti–MAP-2 (1:2,500, M9942; Sigma–Aldrich) antibodies. Samples were imaged on a confocal microscope with a 20× air objective (numerical aperture = 0.5) and pinhole at 1.5 airy units. Cleaved caspase-3–positive neurons were defined as MAP2-positive cells displaying a mean intensity above an intensity threshold in the cleaved caspase-3 channel.

Growth Cone Collapse Assay. Hippocampal neurons were transfected with S6-p75^{NTR}–GFP constructs; alternatively, they were transduced with inducible wt p75^{NTR} or mut p75^{NTR} and induced at 0, 0.05, or 1 μg/mL doxycycline concentrations. On DIV3, p75^{NTR} was biotinylated at the cell surface before incubation with 20 ng/mL proNGF. Neurons were then washed once and incubated with 10 nM streptavidin-Qdot655, washed 5 times, and fixed in 2% formaldehyde and 5% sucrose in PBS before confocal or TIRF imaging. To inhibit p75^{NTR} endocytosis, the above experiment was repeated in the presence of 80 μM Dynasore (Sigma–Aldrich) or 25 μM Pitstop2 (Abcam). We measured 1) the area of all detectable growth cones; 2) for S6-p75^{NTR}–EGFP constructs, the ratio between the Qdot and EGFP channels as a

measure of membrane versus total receptor pool; and 3) for all $p75^{NTR}$ constructs, the intensities in the Qdot channel as a measure of membrane abundance at the different expression levels.

More details on material and methods appear in *SI Appendix*. Readers will be able to access codes and materials by directly contacting the corresponding authors.

ACKNOWLEDGMENTS. We thank Robert Youker for the mut $p75^{NTR}$ construct; Luca Puzzi for the human c-jun complementary DNA, and Gianmichele Ratto for adeno-associated viral vectors for in vivo YFP expression. We thank Carmine Di Rienzo, Francesco Cardarelli, Marco Canossa, Beatrice Vignoli, Michela Serresi, and Andrea Palamidessi for useful discussions. This study was supported by funding from Tuscany Region, Project NOSEISMIC, within Grant POR CRO FSE 2007-2013 (to S.L.); Ministero Università e Ricerca Projects PRIN 2009XPTWM2 (to S.L.) and FIRB RBAP11X42L (to F. Beltram); Fondazione Pisa Project RST 148/16; European Union Paincage and H2020 Human Brain Projects (SGA1 and SGA2) (to A.C.); and Institutional Scuola Normale Superiore funds (to S.L., L.M., and A.C.).

1. M. Vilar, "Structural characterization of the p75 neurotrophin receptor: A stranger in the TNFR superfamily" in *Vitamins and Hormones*, G Litwack, Ed. (Elsevier, 2017), vol. 104, pp. 57–87.
2. E. J. Huang, L. F. Reichardt, Trk receptors: Roles in neuronal signal transduction. *Annu. Rev. Biochem.* **72**, 609–642 (2003).
3. A. Nykjaer, T. E. Willnow, Sortilin: A receptor to regulate neuronal viability and function. *Trends Neurosci.* **35**, 261–270 (2012).
4. M. V. Chao, Neurotrophins and their receptors: A convergence point for many signalling pathways. *Nat. Rev. Neurosci.* **4**, 299–309 (2003).
5. A. Cattaneo, P. Calissano, Nerve growth factor and Alzheimer's disease: New facts for an old hypothesis. *Mol. Neurobiol.* **46**, 588–604 (2012).
6. X. Q. Chen, M. Sawa, W. C. Mobley, Dysregulation of neurotrophin signaling in the pathogenesis of Alzheimer disease and of Alzheimer disease in Down syndrome. *Free Radic Biol. Med.* **114**, 52–61 (2018).
7. B. L. Hempstead, D. Martin-Zanca, D. R. Kaplan, L. F. Parada, M. V. Chao, High-affinity NGF binding requires coexpression of the trk proto-oncogene and the low-affinity NGF receptor. *Nature* **350**, 678–683 (1991).
8. T. Wehrman *et al*., Structural and mechanistic insights into nerve growth factor interactions with the TrkA and p75 receptors. *Neuron* **53**, 25–38 (2007).
9. N. Leloup, L. M. P. Chataigner, B. J. C. Janssen, Structural insights into SorCS2-nerve growth factor complex formation. *Nat. Commun.* **9**, 2979 (2018).
10. P. A. Barker, High affinity not in the vicinity? *Neuron* **53**, 1–4 (2007).
11. X. L. He, K. C. Garcia, Structure of nerve growth factor complexed with the shared neurotrophin receptor p75. *Science* **304**, 870–875 (2004).
12. Y. Gong, P. Cao, H. J. Yu, T. Jiang, Crystal structure of the neurotrophin-3 and p75NTR symmetrical complex. *Nature* **454**, 789–793 (2008).
13. M. Yaar *et al*., Amyloid beta binds trimers as well as monomers of the 75-kDa neurotrophin receptor and activates receptor signaling. *J. Biol. Chem.* **277**, 7720–7725 (2002).
14. K. C. Wang, J. A. Kim, R. Sivasankaran, R. Segal, Z. He, P75 interacts with the Nogo receptor as a co-receptor for Nogo, MAG and OMgp. *Nature* **420**, 74–78 (2002).
15. J. P. Zanin, E. Abercrombie, W. J. Friedman, Proneurotrophin-3 promotes cell cycle withdrawal of developing cerebellar granule cell progenitors via the p75 neurotrophin receptor. *eLife* **5**, e16654 (2016).
16. C. Langevin, H. Jaaro, S. Bressanelli, M. Fainzilber, C. Tuffereau, Rabies virus glycoprotein (RVG) is a trimeric ligand for the N-terminal cysteine-rich domain of the mammalian p75 neurotrophin receptor. *J. Biol. Chem.* **277**, 37655–37662 (2002).
17. M. Vilar *et al*., Activation of the p75 neurotrophin receptor through conformational rearrangement of disulphide-linked receptor dimers. *Neuron* **62**, 72–83 (2009).
18. K. Tanaka, C. E. Kelly, K. Y. Goh, K. B. Lim, C. F. Ibáñez, Death domain signaling by disulfide-linked dimers of the p75 neurotrophin receptor mediates neuronal death in the CNS. *J. Neurosci.* **36**, 5587–5595 (2016).
19. K. S. Mineev, S. A. Goncharuk, P. K. Kuzmichev, M. Vilar, A. S. Arseniev, NMR dynamics of transmembrane and intracellular domains of p75NTR in lipid-protein nanodiscs. *Biophys. J.* **109**, 772–782 (2015).
20. A. Anastasia, P. A. Barker, M. V. Chao, B. L. Hempstead, Detection of p75NTR trimers: Implications for receptor stoichiometry and activation. *J. Neurosci.* **35**, 11911–11920 (2015).
21. L. Marchetti *et al*., Ligand signature in the membrane dynamics of single TrkA receptor molecules. *J. Cell Sci.* **126**, 4445–4456 (2013).
22. T. De Nadai *et al*., Precursor and mature NGF live tracking: One versus many at a time in the axons. *Sci. Rep.* **6**, 20272 (2016).
23. L. Marchetti *et al*., Site-specific labeling of neurotrophins and their receptors via short and versatile peptide tags. *PLoS One* **9**, e113708 (2014).
24. F. Gobbo, F. Bonsignore, R. Amodeo, A. Cattaneo, L. Marchetti, Site-specific direct labeling of neurotrophins and their receptors: From biochemistry to advanced imaging applications. *Methods Mol. Biol.* **1727**, 295–314 (2018).
25. A. Callegari *et al*., Single particle tracking of acyl carrier protein (ACP)-tagged TrkA receptors in PC12nnr5 cells. *J. Neurosci. Methods* **204**, 82–86 (2012).
26. C. Schachtrup *et al*., Nuclear pore complex remodeling by p75(NTR) cleavage controls TGF-β signaling and astrocyte functions. *Nat. Neurosci.* **18**, 1077–1080 (2015).
27. C. K. Underwood, K. Reid, L. M. May, P. F. Bartlett, E. J. Coulson, Palmitoylation of the C-terminal fragment of p75(NTR) regulates death signaling and is required for subsequent cleavage by gamma-secretase. *Mol. Cell. Neurosci.* **37**, 346–358 (2008).
28. E. Zuccaro *et al*., Polarized expression of p75(NTR) specifies axons during development and adult neurogenesis. *Cell Rep.* **7**, 138–152 (2014).
29. K. Deinhardt *et al*., Neuronal growth cone retraction relies on proneurotrophin receptor signaling through Rac. *Sci. Signal.* **4**, ra82 (2011).
30. K. F. Lee *et al*., Targeted mutation of the gene encoding the low affinity NGF receptor p75 leads to deficits in the peripheral sensory nervous system. *Cell* **69**, 737–749 (1992).
31. C. Costantini, R. Weindruch, G. Della Valle, L. Puglielli, A TrkA-to-p75NTR molecular switch activates amyloid beta-peptide generation during aging. *Biochem. J.* **391**, 59–67 (2005).
32. K. Jaqaman *et al*., Cytoskeletal control of CD36 diffusion promotes its receptor and signaling function. *Cell* **146**, 593–606 (2011).
33. R. T. Youker *et al*., Multiple motifs regulate apical sorting of p75 via a mechanism that involves dimerization and higher-order oligomerization. *Mol. Biol. Cell* **24**, 1996–2007 (2013).
34. A. J. Brooks *et al*., Mechanism of activation of protein kinase JAK2 by the growth hormone receptor. *Science* **344**, 1249783 (2014).
35. I. Chung *et al*., Spatial control of EGF receptor activation by reversible dimerization on living cells. *Nature* **464**, 783–787 (2010).
36. R. S. Kasai, A. Kusumi, Single-molecule imaging revealed dynamic GPCR dimerization. *Curr. Opin. Cell Biol.* **27**, 78–86 (2014).
37. W. Zhang *et al*., Single-molecule imaging reveals transforming growth factor-β-induced type II receptor dimerization. *Proc. Natl. Acad. Sci. U.S.A.* **106**, 15679–15683 (2009).
38. A. M. Sykes *et al*., The effects of transmembrane sequence and dimerization on cleavage of the p75 neurotrophin receptor by γ-secretase. *J. Biol. Chem.* **287**, 43810–43824 (2012).
39. K. Simons, J. L. Sampaio, Membrane organization and lipid rafts. *Cold Spring Harb. Perspect. Biol.* **3**, a004697 (2011).
40. Z. Korade, A. K. Kenworthy, Lipid rafts, cholesterol, and the brain. *Neuropharmacology* **55**, 1265–1273 (2008).
41. F. C. Bronfman, O. M. Lazo, C. Flores, C. A. Escudero, Spatiotemporal intracellular dynamics of neurotrophin and its receptors. Implications for neurotrophin signaling and neuronal function. *Handb. Exp. Pharmacol.* **220**, 33–65 (2015).
42. M. P. J. Dekkers, V. Nikoletopoulou, Y. A. Barde, Cell biology in neuroscience: Death of developing neurons: New insights and implications for connectivity. *J. Cell Biol.* **203**, 385–393 (2013).
43. C. A. Day, A. K. Kenworthy, Tracking microdomain dynamics in cell membranes. *Biochim. Biophys. Acta Biomembr.* **1788**, 245–253 (2009).
44. Y. H. Zhang, R. Khanna, G. D. Nicol, Nerve growth factor/p75 neurotrophin receptor-mediated sensitization of rat sensory neurons depends on membrane cholesterol. *Neuroscience* **248**, 562–570 (2013).
45. C. S. Huang *et al*., Nerve growth factor signaling in caveolae-like domains at the plasma membrane. *J. Biol. Chem.* **274**, 36707–36714 (1999).
46. F. Pinaud *et al*., Dynamic partitioning of a glycosyl-phosphatidylinositol-anchored protein in glycosphingolipid-rich microdomains imaged by single-quantum dot tracking. *Traffic* **10**, 691–712 (2009).
47. N. Komura *et al*., Raft-based interactions of gangliosides with a GPI-anchored receptor. *Nat. Chem. Biol.* **12**, 402–410 (2016).
48. J. M. Frade, A. Rodríguez-Tébar, Y. A. Barde, Induction of cell death by endogenous nerve growth factor through its p75 receptor. *Nature* **383**, 166–168 (1996).
49. S. X. Bamji *et al*., The p75 neurotrophin receptor mediates neuronal apoptosis and is essential for naturally occurring sympathetic neuron death. *J. Cell Biol.* **140**, 911–923 (1998).
50. M. Zagrebelsky *et al*., The p75 neurotrophin receptor negatively modulates dendrite complexity and spine density in hippocampal neurons. *J. Neurosci.* **25**, 9989–9999 (2005).
51. L. Cognet, B. Lounis, D. Choquet, Tracking receptors using individual fluorescent and nonfluorescent nanolabels. *Cold Spring Harb. Protoc.* **2014**, 207–213 (2014).
52. T. Yamashita, H. Higuchi, M. Tohyama, The p75 receptor transduces the signal from myelin-associated glycoprotein to Rho. *J. Cell Biol.* **157**, 565–570 (2002).
53. A. K. Lewis *et al*., Death receptor 5 networks require membrane cholesterol for proper structure and function. *J. Mol. Biol.* **428**, 4843–4855 (2016).
54. P. M. Dijkman *et al*., Dynamic tuneable G protein-coupled receptor monomer-dimer populations. *Nat. Commun.* **9**, 1710 (2018).
55. P. Mehlen, C. Thibert, Dependence receptors: Between life and death. *Cell. Mol. Life Sci.* **61**, 1854–1866 (2004).
56. K. D. Nadezhdin *et al*., Structural basis of p75 transmembrane domain dimerization. *J. Biol. Chem.* **291**, 12346–12357 (2016).
57. Y. S. Lim *et al*., p75(NTR) mediates ephrin-A reverse signaling required for axon repulsion and mapping. *Neuron* **59**, 746–758 (2008).
58. S. Glerup *et al*., SorCS2 regulates dopaminergic wiring and is processed into an apoptotic two-chain receptor in peripheral glia. *Neuron* **82**, 1074–1087 (2014).
59. N. K. Dhanoa, K. M. Krol, A. Jahed, K. A. Crutcher, M. D. Kawaja, Null mutations for exon III and exon IV of the p75 neurotrophin receptor gene enhance sympathetic sprouting in response to elevated levels of nerve growth factor in transgenic mice. *Exp. Neurol.* **198**, 416–426 (2006).
60. E. E. Zahavi *et al*., The receptor tyrosine kinase TrkB signals without dimerization at the plasma membrane. *Sci. Signal.* **11**, eaao4006 (2018).
61. S. Covaceuszach *et al*., The conundrum of the high-affinity NGF binding site formation unveiled? *Biophys. J.* **108**, 687–697 (2015).